

Berezinskii-Kosterlitz-Thouless phase induced by dissipating quasisolitons

Krzysztof Gawryluk¹ and Mirosław Brewczyk¹

¹ *Wydział Fizyki, Uniwersytet w Białymstoku, ul. K. Ciołkowskiego 1L, 15-245 Białystok, Poland*

(Dated: January 17, 2022)

Intrigued by a recent experiment [J.L. Ville et al., Phys. Rev. Lett. 121, 145301 (2018)], we study the sound propagation in a two-dimensional weakly interacting uniform Bose gas. Using the classical fields approximation we first successfully reproduce original experimental results and next, we analyze in detail the nature of generated density waves. Playing with a spatial resolution of our (numerical) imaging system, we identify observed structures as quasisolitons and uncover their internal complexity. Quasisolitons break into vortex pairs as time progresses, eventually reaching an equilibrium state. We find this state, characterized by only fluctuating in time averaged number of pairs of opposite charge vortices and by appearance of quasi-long-range order, as the Berezinskii-Kosterlitz-Thouless (BKT) phase.

Sound waves carry information on both thermodynamic and transport properties of a medium they propagate through. In classical hydrodynamics, measuring the speed of sound waves and their attenuation gives an access to characteristics of the medium such as the compressibility and viscosity. In quantum hydrodynamics, with superfluids present, the picture is more complex [1]. For example, liquid helium and weakly interacting Bose gas respond to local perturbation in a qualitatively different ways.

Many experiments exploring the phenomenon of sound propagation in ultracold atomic systems have been already performed. Sound waves were studied in harmonically trapped three-dimensional bosonic gases at very low [2, 3] as well as at higher [4] temperatures. Sound velocity was measured at resonance in a mixture of fermionic lithium atoms [5]. Two sound modes propagating at different speeds, according to predictions of two-fluid hydrodynamics, were observed in a resonant Fermi gas [6]. The sound diffusion in a unitary three-dimensional Fermi gas was investigated and a universal quantum limit of diffusivity was observed in Ref. [7]. Recently, sound propagation and damping were studied in two-dimensional systems – a weakly interacting Bose [8, 9] and strongly interacting Fermi [10] gases.

In [8], a gas of rubidium-87 atoms is confined inside a quasi-2D rectangular potential with hard walls. A density perturbation is introduced by applying a repulsive potential to the cloud of atoms. This additional potential creates a density dip along one direction which propagates at constant speed when the laser is switched off. During this evolution the density perturbation bounces several times off the walls of the box and its velocity is found to be close to the Bogoliubov sound speed. Several attempts have been already undertaken to reproduce results of this experiment [11–13]. They all support experimental observation that below the BKT transition the generated sound waves propagate with velocities close to the speed of second sound, predicted by two-fluid hydrodynamic model. They also predict that sound waves can propagate above the BKT transition, in agreement with experiment and in opposition to what is predicted by two-fluid hydrodynamic model with respect to second

sound [14, 15].

In our numerical simulations we first model the experiment [8]. With the help of Metropolis algorithm [13, 16–21] we create an ensemble of initial states, $\psi(\mathbf{r})$, for a two-dimensional Bose gas confined in a box potential with periodic boundary conditions. We do this for various temperatures in order to have temperature-dependent analysis. Next, we follow a disturbance protocol described in [8]: we create a dip in density in one direction. This dip is characterized by two parameters: the width (w) and the depth (d). Such disturbance, a kind of density imprinting, is then evolved according to the classical field approximation (CFA) equations [22]. In our case the perturbation is initially located at the center of the box, not on a side of it. As a consequence we have two density patterns propagating symmetrically outward as in the experiment of [2], not only in one direction as in the original setup. Integrating density along the direction transverse to the sound propagation we are able to identify traveling waves and compare their speeds to experimental values. In Fig. 1 we show results, coming from our simulations, corresponding to the one presented in Fig. 1 of Ref. [8] (the interaction strength $g = 0.16 \hbar^2/m$, the temperature $T/T_c = 0.37$, where $T_c = 2\pi n \hbar^2 / [m k_B \ln(380 \hbar^2/mg)]$ [23], and the two-dimensional density is $n = 29 \mu\text{m}^{-2}$).

Our numerical experiment resembles the real one [8] – initial central depletion (which in our case splits into two density dips) evolves with a constant speed. Already early stages of the evolution are enough to determine the velocity of a density wave. In Fig. 1 we show the response of the system to two perturbations: the depth of a density dip is the same in both cases and equals about 1/3 of an unperturbed density and the width is $w = 0.25$ ($w = 0.1$) for upper (lower) frame, in units of the box length L . Hence, upper frame corresponds to Fig. 1 in [8]. It turns out that density dips propagate with very similar velocities, $v = 71.2 \hbar/mL$ ($v = 72.4 \hbar/mL$) for upper (lower) case. Simultaneously, the Bogoliubov speed calculated as $c_B = \sqrt{gN/L^2m}$ equals $c_B = 79.2 \hbar/mL$ since the number of atoms remaining in the box after switching off blue laser is $N = 39234$ for the upper frame and $c_B = 81.3 \hbar/mL$ for lower frame (here, the number of remaining atoms is 41372). In both cases the resulting

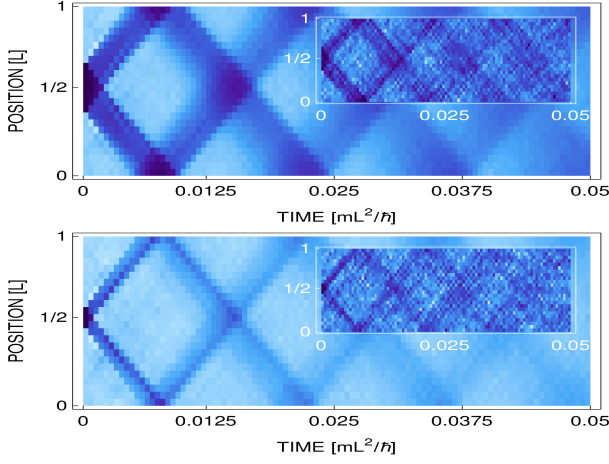


FIG. 1: Propagation of sound waves in a box potential. Here, at each time two-dimensional density is integrated along the direction perpendicular to the sound propagation and then averaged over a hundred realizations. The effective one-dimensional density is shown as a function of time. The width of the density depletion equals $w = 0.25$ (upper frame) and $w = 0.1$ (lower frame) both in units of the box length L , and the depth of a density dip is $5/16$ of initial density ($N = 42275$ in both cases). The temperature is $T = 0.37T_c$. Total evolution time $t = 0.05 mL^2/\hbar$ corresponds to 100 ms for $L = 38\mu m$. Insets present a single realization results. The spatial resolution here is $0.76\mu m$ which is 1.58 of the healing length $\xi = \hbar/\sqrt{mng}$.

density waves are traveling with velocities close to the Bogoliubov sound speed ($v = 0.90c_B$ in the first case and $v = 0.89c_B$ in the second). These two examples might suggest that the velocity of created density dips do not depend on details of perturbation. However, as discussed below, this is not the case – stronger initial disturbance actually decreases the speed of a density wave.

To get the velocities of density waves we follow the procedure presented in the experimental paper: we decompose the density integrated along the direction perpendicular to the wave propagation, let's say y axis, via the Fourier transform at each instant of time

$$n(x, t) = \langle n \rangle + \sum_{j=\pm 1, \pm 2, \dots} A_j(t) \exp(j 2\pi x/L), \quad (1)$$

where $\langle n \rangle$ is the average density along x axis. Then we do time analysis of $A_j(t)/A_j(0)$ coefficients – we fit real (or imaginary) part of them to an exponentially damped sinusoidal function

$$e^{-\Gamma_j t/2} [\Gamma_j/(2\omega_j) \sin(\omega_j t) + \cos(\omega_j t)]. \quad (2)$$

Focusing on lower energy modes we obtain the velocity of density waves as $v = \omega_j/k_j$, where k_j is the wave vector ($k_j = \pm j 2\pi/L$, since periodic boundary conditions are applied in our case). For data presented in Fig. 1 lower energy modes lead to almost the same velocity v .

In Fig. 2 we summarize our results. Two sets of equilibrium states, corresponding to different values of chemical potential (as indicated in the legend), are used for

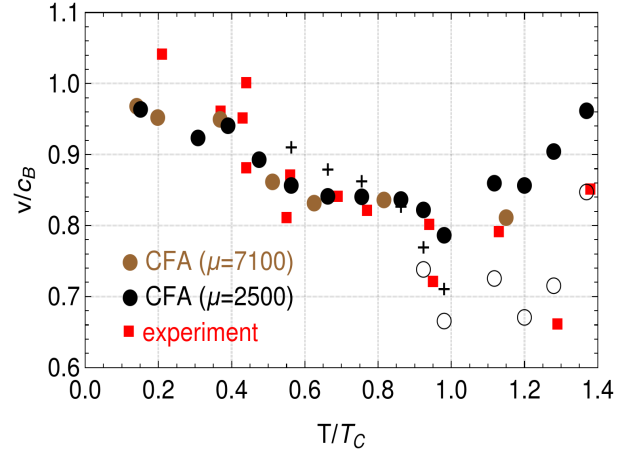


FIG. 2: Speed of sound normalized to the Bogoliubov sound speed (at zero temperature) shown as a function of T/T_c . Black and brown bullets (obtained at different values of chemical potential, in units of \hbar^2/mL^2 , as indicated in the legend) come from numerical simulations whereas red squares are experimental results [8]. Numerical results are obtained within weak perturbation scheme, with $w \approx 0.25$ and $d \lesssim 5/16$. Open circles represent numerical data for stronger disturbance, $w < 0.25$ and $d \gg 5/16$. Crosses are the outcome of two-fluid model [1, 14], showing the speed of second sound.

the analysis. Numerical values of the speed of sound waves (black and brown bullets, black circles) remain in a good agreement with experimental data (red squares) in the whole range of studied temperatures [8]. Most of the data in Fig. 2 were obtained assuming a density imprinting parameters: $w = 0.25$ and $d = 5/16$ (as in the case of Fig. 1 in [8]). Some of the points (brown bullets) were calculated in the regime of very weak perturbation, $d = 1/16$. Close to the transition and for the normal phase we double results showing also the response of the system to stronger initial disturbance (black circles, for which $d \gg 5/16$). Numerical data clearly demonstrate that the response of the system depends on the strength of initial density imprinting. Similar observation was reported in Ref. [3], where the wave fronts propagation through the condensate was studied after it was split by a strong laser beam. The reason why the authors of Ref. [8] do not observe such a dependence, we believe, is mostly related to the spatial resolution of the imaging system they use.

Additionally, we put in Fig. 2 values of the speed of second sound, coming from the two-fluid model [1, 14, 15]. Within this framework one can calculate a value of the speed of second sound, c_2 , from the equation

$$c^4 - \left(\frac{1}{mn\kappa_S} + \frac{n_s T \tilde{s}^2}{n_n \tilde{c}_V} \right) c^2 + \frac{n_s T \tilde{s}^2}{n_n \tilde{c}_V} \frac{1}{mn\kappa_T} = 0, \quad (3)$$

where n_s , n_n , and $n (= n_s + n_n)$ are superfluid, normal, and total densities, respectively. κ_T (κ_S) is the isothermal (adiabatic) compressibility, \tilde{s} is the entropy, and \tilde{c}_V – the specific heat at constant volume, both per unit mass.

For temperatures such that $k_B T > gn$, a good approximation to the velocity of second sound is given by the expression $c_2 = \sqrt{n_s/n}/\sqrt{mn\kappa_T}$ [14]. Within CFA we can calculate both the superfluid density (from current-current correlations [21]) and the isothermal compressibility. The latter is obtained from the fluctuation-dissipation relation $(\langle N^2 \rangle - \langle N \rangle^2)/\langle N \rangle^2 = k_B T \kappa_T/V$ [24]. The speed of second sound, as a function of T/T_c , is plotted in Fig. 2 by black crosses and the values are close to experimental (and CFA) results.

In CFA approach the classical field is expanded in the basis of modes which are macroscopically occupied – in our case these are simply the plane waves [22]. Dynamical equations for modes amplitudes (expansion coefficients) can be written in the form of a set of nonlinear differential equations. At each instant of time, these amplitudes determine fully the classical field. Hence, we can watch the density (square modulus of the classical field) with arbitrary high spatial resolution. In particular, this resolution can be high enough to resolve the healing length scale, not accessible in the experiment [8].

Indeed, with high resolution employed, new observations are possible. In particular, interesting things happen when the density imprinting parameters, the width (w) and the depth (d) of the initial depletion region, are being significantly changed. For some choice of these parameters we note that the response of the system starts to differ, which is in contrary to what is reported in [8]. First of all, we find that the visible density waves, in fact, consist of several thinner structures, which are characterized by slightly different velocities, see Fig. 3. Only for weak initial perturbations (both in the width and depth; $d \gtrsim 14/16$) they travel with the same speed and form a single beam (as in Fig. 1), provided low spatial resolution is used for imaging. Moreover, for the same width and bigger depth of initial disturbance we clearly see signs of nonlinear behavior – lines in time-position plots (Fig. 3, right column) are no longer straight. Also, internal structures separate each other and travel with slightly different velocities. To conclude, stronger initial perturbation leads to nonlinear effects – multiple density dips travel with different velocities, yet accelerate during the motion. At the same time, larger the width of initial perturbation w bigger the number of created waves. Such behavior can not be described by an approach of Ref. [11], combining the Boltzmann transport equation with linear response theory as well as by direct solution of the linearized Landau-Vlasov equation as in Ref. [12].

In Fig. 3 we apply the spatial resolution equal to 1.0ξ , where ξ is the healing length. In the experiment [8] the size of a single CCD camera pixel is $1.18\mu\text{m}$ [25], i.e. 2.46ξ for the case of Fig. 3. This is certainly not high enough resolution to distinguish structures we show in Fig. 3, right column. Experimental resolution enables to observe the response of the system only in a form of a single line (in time-position plots).

The number of internal thin waves visible inside broad dips in Fig. 3 is well described by the formula $w/(4\xi)$,

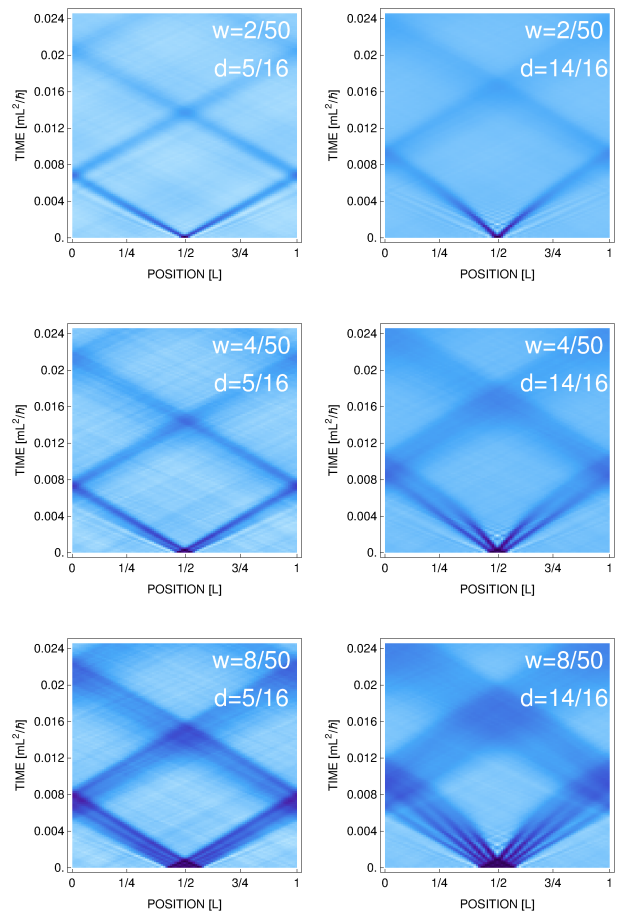


FIG. 3: Time evolution of initially perturbed equilibrium state. Two-dimensional density of the system is first integrated along one direction, next averaged over approximately 100 realizations, and then shown as a function of time. Perturbation parameters, the width (w) and depth (d) are given in the frames. Temperature is $T = 0.37T_c$. Total evolution time $t = 0.025 mL^2/\hbar$ corresponds to 50 ms for $L = 38\mu\text{m}$. Here, the spatial resolution is the healing length.

where w is the width of initial perturbation. Factor 4 arises from a typical width of these structures, see Fig. 3, which turns out to be about 4ξ .

Structures presented in Fig. 1 and 3 survive several crossings and exhibit a moderate change of shapes during the evolution, so one can try to assign some solitonic properties to them. Below we examine numerically obtained densities by comparing their profiles with analytical formulas for a single soliton solution of a nonlinear Schrödinger equation, known as Zakharov-Shabat solutions with the nonlinear term corresponding to repulsive interactions [26]

$$|\phi_{ZS}(x, t)|^2 = n_0 \left[\frac{\dot{q}^2}{c_B^2} + \left(1 - \frac{\dot{q}^2}{c_B^2} \right) \tanh^2 \left(\frac{x - q}{\xi} \sqrt{1 - \frac{\dot{q}^2}{c_B^2}} \right) \right]. \quad (4)$$

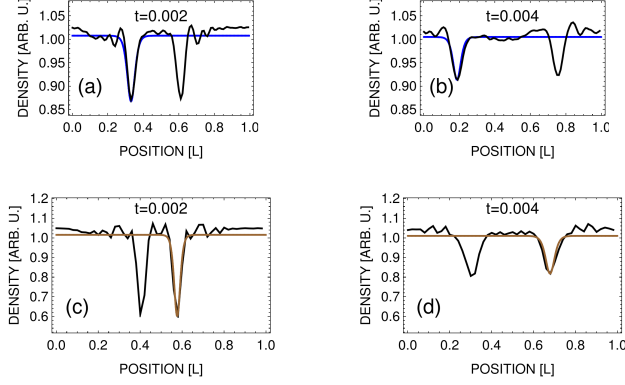


FIG. 4: Upper row: Density cuts for weak initial perturbation ($w = 2/50, d = 5/16$, which corresponds to the first frame in Fig. 3) together with fits according to dissipative Zakharov-Shabat solution, Eq. (5), for different times. For frames (a) and (b), i.e. before the first collision, $\Gamma = 126$ and $\Gamma = 169$, respectively. Lower row: Density cuts for stronger initial perturbation ($w = 2/50, d = 14/16$, which corresponds to the second frame in Fig. 3) together with fits according to “accelerating” solutions of Eq. (4), for different times ($\dot{q} = 0.77 c_B$ for (c) and $\dot{q} = 0.90 c_B$ for (d)).

Here, n_0 is the density of the medium far away from the soliton dip, q and \dot{q} are the position and velocity of the soliton, respectively. The healing length $\xi = \hbar/\sqrt{mn_0g}$ and $c_B = \sqrt{n_0g/m}$. The width and the depth of solitonic solution (4) is solely determined by soliton velocity, \dot{q} . For weak perturbations (upper left frame in Fig. 3) density dips propagate with constant velocity but they get shallower in time (due to snake instabilities [27–31]). Hence, additional damping factor has to be included in Eq. (4) and then a dissipative Zakharov-Shabat solution takes the form

$$|\psi(x, t)|^2 = \exp(-\Gamma(t)t) |\phi_{ZS}(x, t)|^2. \quad (5)$$

On the other hand, for strong perturbations (right column in Fig. 3) the density waves accelerate in time. In this case, the parameter \dot{q} in Eq. (4) should depend on time.

To verify this concept we analyze first the simplest case – a small initial perturbation in both w and d which leads to single wave moving with constant velocity. In Fig. 4, frames (a) and (b), we compare numerically obtained density cuts for various times with Eq. (5), where \dot{q} is fixed by the value of v we get from the time-dependent analysis of $A_1(t)$ coefficient (from Eq. (2) we have $v = 74.45 \hbar/mL = 0.90 c_B$). It turns out that both densities match perfectly up to first collision, after which the agreement slowly degrades. Surprisingly, Eq. (4) works well also for strong perturbation, although in this case one has to consider rather an accelerating soliton solutions of (4), i.e. a solution with time-dependent \dot{q} . Frames (c) and (d) prove that an agreement is good, here $w = 2/50$ and $d = 14/16$. Hence, we will be naming ob-

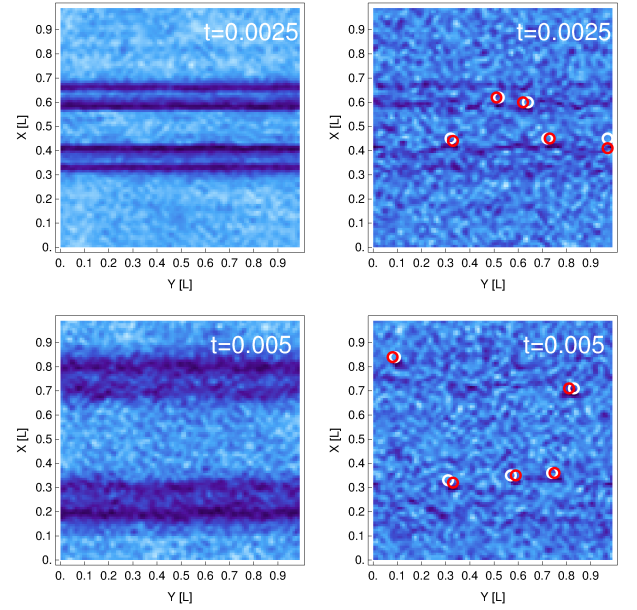


FIG. 5: Left column: 2D time-snapshots of a density (averaged over 170 realizations) for $t = 0.0025$ and $t = 0.005$. Right column: 2D density for a single realization, with marked circles surrounding vortex pairs. Here, $w = 4/50, d = 14/16$, and $T = 0.37T_c$, which corresponds to the middle right frame in Fig. 3. The spatial resolution here is $0.76\mu\text{m}$ which is 1.58 of the healing length.

served structures as quasisolitons. Surprisingly, Eq. (4) also works for weak perturbations at longer times, i.e. after first collision of density waves. Density dips become, as time progresses, broader and shallower and their velocity increases towards speed of Bogoliubov sound (similarly to dissipative dynamics of solitons already observed in early experiments on dark solitons created by phase imprinting technique [32] and theoretically discussed in [33]).

As observed in simulations, quasisolitons dissipate and eventually break into vortex pairs. It is illustrated in Fig. 5, right column, where densities for single realizations are shown. Almost no trace of density waves is visible, although, while averaged over a hundred realizations, density dips are still there (left column). Additionally, positions of pairs of opposite charge vortices are marked by color circles. The number of vortex pairs changes in time but finally a thermal equilibrium is established, see Fig. 6 (lower frame), exhibiting only fluctuating, after averaging over a hundred realizations, number of vortex pairs. The final number of vortex pairs depends on the strength of initial density perturbation, the stronger disturbance the larger number of pairs.

Production of vortex-antivortex pairs in two-dimensional condensates, due to snake instability of initially imprinted dark soliton, was thoroughly discussed in [34]. As demonstrated theoretically in [35], creation of vortex-antivortex pairs is expected to occur in a laser-stirred two-dimensional Bose gas, as

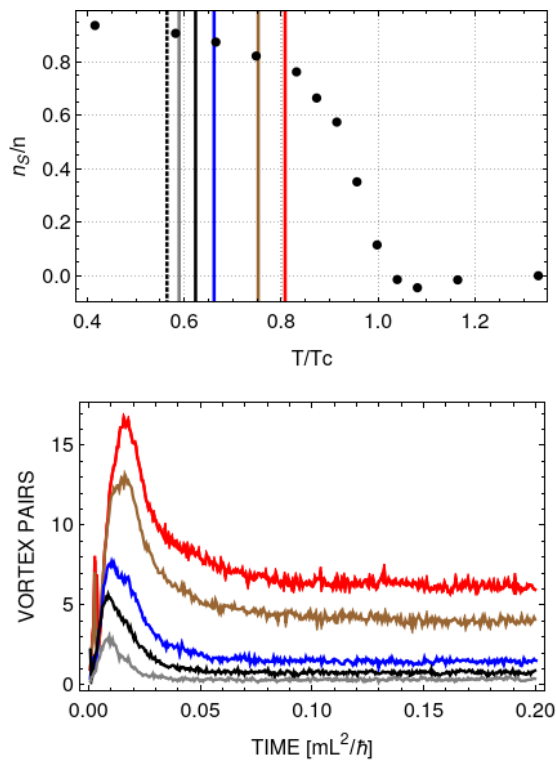


FIG. 6: Upper frame: Superfluid fraction as a function of temperature (black dots) for $\mu = 2500 \hbar^2/mL^2$ (from [21]). Initially, i.e. before perturbation, the system is prepared at temperature $T/T_c = 0.56$ (vertical dotted line, most left). After density imprinting with the depth $d = 14/16$ and the widths $w = (2, 4, 8, 10, 12)/34$ the system's relative temperature is shifted up (shown by successive vertical lines). Lower frame: number of pairs of opposite charge vortices (averaged over 100 realizations) versus time, for various perturbations as in upper frame. Stronger perturbation leads to larger number of vortices at equilibrium, i.e. at longer times. Total evolution time $t = 0.20 mL^2/\hbar$ corresponds to 400 ms for $L = 38 \mu m$.

in the experiment of [36]. There, an additional energy is pumped into the system due to stirring the gas. Increasing energy, after thermalization, results in higher temperature of the system and makes the system to be closer to the transition point. Hence, pairs of opposite sign vortices should appear in the gas as predicted by the BKT theory [37, 38].

In experiment [8], as opposed to [36], the energy of the system is preserved during the evolution. In numerical simulations, we initially prepare the sample of undisturbed Bose gas and next we remove suddenly some part

of the atomic cloud. Hence, in our case the total energy of the system is even decreased but the energy per particle is preserved. However, a two-dimensional Bose gas is shifted towards the transition point because the transition temperature is reduced (since the atomic density gets lower, see [23]). Indeed, as visible in Fig. 6, the number of vortex pairs increases with the strength of perturbation. Upper frame in Fig. 6 shows effective ratio T/T_c after disturbance. Occurrence of vortices could be related to the appearance of the BKT phase [39, 40]. To clarify the situation we calculate the first-order correlation function $g^{(1)}(\mathbf{r}, \mathbf{r}')$, defined as a normalized average $g^{(1)}(\mathbf{r}, \mathbf{r}') = \langle \psi^*(\mathbf{r}) \psi(\mathbf{r}') \rangle / \langle \psi^*(\mathbf{r}) \rangle \langle \psi(\mathbf{r}') \rangle$ over the grand canonical ensemble, while the system evolves. We find that at $t \approx 0.05 mL^2/\hbar$ the first-order correlation function already decays algebraically, although with different exponents in x and y directions. However, for $t \gtrsim 0.10 mL^2/\hbar$ the system starts exhibiting the quasi-long-range order, i.e. $g^{(1)}(\mathbf{r}, 0)$ drops algebraically with a distance, here with exponent equal to ≈ 0.13 . Hence, the system enters the BKT phase.

In summary, following a recent experiment [8], we have studied the propagation of sound in a two-dimensional weakly interacting uniform Bose gas. The velocities of density waves, we obtain from numerical simulations, agree with the experimentally measured (see Fig. 2). We find, however, that the response of the system is much richer than reported in Ref. [8]. Indeed, we identify patterns of multiple density dips, propagating with slightly different velocities, when stronger disturbance of initial state is chosen. Size of these structures is of submicron and their shape coincides with dissipative Zakharov-Shabat profile. These structures (quasisolitons) dissipate, changing into pairs of opposite charge vortices. Finally, the equilibrium is reached and the system enters the BKT phase at higher T/T_c ratio. Such an induced BKT phase appears here not because an additional energy is pumped into the system but rather because the critical temperature is reduced since the atomic density is depleted.

Acknowledgments

We are grateful to P. Deuar, M. Gajda, and K. Rzażewski for helpful discussions. Part of the results were obtained using computers at the Computer Center of University of Białystok.

[1] L. Pitaevskii and S. Stringari, *Bose-Einstein Condensation* (Oxford University Press, Oxford, 2003).
[2] M.R. Andrews, D. M. Kurn, H.-J. Miesner, D.S. Durfee, C. G. Townsend, S. Inouye, and W. Ketterle, Phys. Rev. Lett. **79**, 553 (1997).

[3] J.J. Chang, P. Engels, and M.A. Hoefer, Phys. Rev. Lett. **101**, 170404 (2008).
[4] R. Meppelink, S.B. Koller, and P. van der Straten, Phys. Rev. A **80**, 043605 (2009).
[5] J. Joseph, B. Clancy, L. Luo, J. Kinast, A. Turlapov, and

- J.E. Thomas, Phys. Rev. Lett. **98**, 170401 (2007).
- [6] L.A. Sidorenkov, M.K. Tey, R. Grimm, Y.H. Hou, L. Pitaevskii, and S. Stringari, Nature (London) **498**, 78 (2013).
- [7] P.B. Patel, Z. Yan, B. Mukherjee, R.J. Fletcher, J. Struck, and M.W. Zwierlein, arXiv:1909.02555v2.
- [8] J.L. Ville, R. Saint-Jalm, É. Le Cerf, M. Aidelsburger, S. Nascimbène, J. Dalibard, and J. Beugnon, Phys. Rev. Lett. **121**, 145301 (2018).
- [9] P. Christodoulou, M. Galka, N. Dogra, R. Lopes, J. Schmitt, and Z. Hadzibabic, arXiv:2008.06044v1.
- [10] M. Bohlen, L. Sobirey, N. Luick, H. Biss, T. Enss, T. Lompe, and H. Moritz, Phys. Rev. Lett. **124**, 240403 (2020).
- [11] M. Ota, F. Larcher, F. Dalfovo, L. Pitaevskii, N.P. Proukakis, and S. Stringari, Phys. Rev. Lett. **121**, 145302 (2018).
- [12] A. Cappellaro, F. Toigo, and L. Salasnich, Phys. Rev. A **98**, 043605 (2018).
- [13] V.P. Singh and L. Mathey, Phys. Rev. Res. **2**, 023336 (2020).
- [14] T. Ozawa and S. Stringari, Phys. Rev. Lett. **112**, 025302 (2014).
- [15] M. Ota and S. Stringari, Phys. Rev. A **97**, 033604 (2018).
- [16] E. Witkowska, M. Gajda, and K. Rzążewski, Opt. Commun. **283**, 671 (2010).
- [17] P. Grišins and I.E. Mazets, Comput. Phys. Comm. **185**, 1926 (2014).
- [18] T. Karpiuk, T. Sowiński, M. Gajda, K. Rzążewski, and M. Brewczyk, Phys. Rev. A **91**, 013621 (2015).
- [19] J. Pietraszewicz and P. Deuar, Phys. Rev. A **92**, 063620 (2015).
- [20] K. Gawryluk, M. Brewczyk, and K. Rzążewski, Phys. Rev. A **95**, 043612 (2017).
- [21] K. Gawryluk and M. Brewczyk, Phys. Rev. A **99**, 033615 (2019).
- [22] M. Brewczyk, M. Gajda, and K. Rzążewski, J. Phys. B **40**, R1 (2007).
- [23] N. Prokof'ev, O. Ruebenacker, and B. Svistunov, Phys. Rev. Lett. **87**, 270402 (2001).
- [24] K. Huang, *Statistical Mechanics* (Wiley, Delhi, 2014).
- [25] J. Beugnon, private communication.
- [26] V.E. Zakharov and A.B. Shabat, Zh. Eksp. Teor. Fiz. **64**, 1627 (1973) [Sov. Phys. JETP **37**, 823 (1973)].
- [27] B.P. Anderson, P.C. Haljan, C.A. Regal, D.L. Feder, L.A. Collins, C.W. Clark, and E.A. Cornell, Phys. Rev. Lett. **86**, 2926 (2001).
- [28] Z. Dutton, M. Budde, C. Slowe, and L.V. Hau, Science **293**, 663 (2001).
- [29] D.L. Feder, M.S. Pindzola, L.A. Collins, B.I. Schneider, and C.W. Clark, Phys. Rev. A **62**, 053606 (2000).
- [30] S. Tsuchiya, F. Dalfovo, and L. Pitaevskii, Phys. Rev. A **77**, 045601 (2008).
- [31] H. Ohya, S. Watanabe, and T. Nikuni, J. Low Temp. Phys. **196**, 140 (2019).
- [32] S. Burger, K. Bongs, S. Dettmer, W. Ertmer, K. Sengstock, A. Sanpera, G.V. Shlyapnikov, and M. Lewenstein, Phys. Rev. Lett. **83**, 5198 (1999).
- [33] P.O. Fedichev, E. Muryshev, and G.V. Shlyapnikov, Phys. Rev. A **60**, 3220 (1999).
- [34] G. Verma, U.D. Rapol, and R. Nath, Phys. Rev. A **95**, 043618 (2017).
- [35] V.P. Singh, C. Weitenberg, J. Dalibard, and L. Mathey, Phys. Rev. A **95**, 043631 (2017).
- [36] R. Desbuquois, L. Chomaz, T. Yefsah, J. Léonard, J. Beugnon, C. Weitenberg, and J. Dalibard, Nat. Phys. **8**, 645 (2012).
- [37] J.M. Kosterlitz and D.J. Thouless, J. Phys. C **6**, 1181 (1973).
- [38] J.M. Kosterlitz, J. Phys. C **7**, 1046 (1974).
- [39] Z. Hadzibabic, P. Krüger, M. Cheneau, B. Battelier, and J. Dalibard, Nature **441**, 1118 (2006).
- [40] L. Chomaz, L. Corman, T. Bienaimé, R. Desbuquois, C. Weitenberg, S. Nascimbène, J. Beugnon, and J. Dalibard, Nat. Commun. **6**, 6162 (2015).